# High surface area stainless steel wire mesh-supported $TiO_2$ prepared by sacrificial template accelerated hydrolysis. A monolithic photocatalyst superior to P25 $TiO_2$

Tan T.Vu, Teresa Valdés-Solís and Gregorio Marbán♣

*Instituto Nacional del Carbón (INCAR-CSIC) – c/Francisco Pintado Fe 26, 33011-Oviedo (Spain). Tel. +34 985119090; Fax +34 985297662*

ARTICLE PUBLISHED IN JOURNAL OF ENVIRONMENTAL CHEMICAL ENGINEERING 2 (4) 2229-2235

## Abstract

High surface area stainless steel wire mesh-supported $TiO_2$ catalysts were prepared by sacrificial template accelerated hydrolysis using highly polar stainless steel wire mesh-supported ZnO templates. The monolithic catalysts were tested for the photodegradation of methylene blue in aqueous solution under ultraviolet irradiation. The calcination temperature of the catalysts was observed to have a determinant effect on their catalytic activity. The optimum calcination temperature range was 450-600°C, in which a combination of high surface area (50-90 $m^2$ $g^{-1}$), a high degree of crystallinity and a minimum rutile content yielded the best catalytic results, with maximum catalytic activity appearing for a calcination temperature of 450°C. The most active catalyst prepared in this work displayed twice the catalytic activity of the reference catalyst, P25 $TiO_2$.

**Keywords:** $TiO_2$, sacrificial template, photodegradation, methylene blue, P25 $TiO_2$

♣ Corresponding author: greca@incar.csic.es

## 1. Introduction

Titania ($TiO_2$) is considered to be one of the most useful semiconducting metal oxides and is employed in applications ranging from sensors to photonic crystals [1], energy storage [2, 3], solar cells [4], micro-optoelectronics [5] and photocatalysis [3]. Its band gap energy (Eg=3.2 eV) allows the absorption of UV light, generating electrons ($e^-$) and holes ($h^+$), which can subsequently induce redox reactions for the degradation of organics in wastewaters. $TiO_2$ offers a number of advantages, including its low cost, relatively high photocatalytic activity, low toxicity and high chemical stability [6]. It has been established that the $TiO_2$ material must have a highly crystalline structure to enhance the generation and migration of photogenerated electrons/holes [7]. A high specific surface area is also of critical importance for increasing the number of redox reaction sites on the catalyst surface. $TiO_2$ has three main crystalline phases: brookite, anatase, and rutile, of which the last two are photocatalytically active. Although rutile has lower band gap energy than anatase, from a photocatalytic point of view anatase is undoubtedly the more active phase due to its higher reduction potential and lower re-combination rate of electron-hole pairs. A highly crystallized anatase phase material with a small grain size and elevated surface area is therefore the preferred combination for $TiO_2$-based photocatalysts [8-10]. Calcination at high temperatures is a simple method to induce the crystallization of amorphous $TiO_2$ produced from sol-gel processes. Typically, amorphous $TiO_2$ is first transformed into small crystals of metastable anatase, which grow upon continuous heating, and then change to rutile crystals as the temperature increases [11]. Crystallization from amorphous $TiO_2$ to anatase and then from anatase to rutile usually occurs in the temperature ranges of 450-550°C and 600-700°C, respectively.

These properties (high surface area and crystallinity) are clearly apparent in the well-known commercial $TiO_2$ material Aeroxide® P25 $TiO_2$, which is a reference material in most works dealing with catalytic photodegradation of organics in wastewaters. P25 $TiO_2$ has around 87 wt.% anatase and 13 wt.% rutile, a crystal size of about 20 nm and a specific surface area of around 55 $m^2 g^{-1}$ [12]. However, P25 $TiO_2$ shares the common disadvantage of all particulate materials, i.e. it has to be separated from the reaction medium by means of energy-consuming methods. According to Evonik, the company that fabricates P25 $TiO_2$, *handling AEROXIDE® Fumed Metal Oxides such as "P25" requires sophisticated handling due to the fineness and fluffy nature of the powder* (source: www.evonik.de). To circumvent this drawback it is necessary to find suitable monolithic configurations for $TiO_2$. $TiO_2$ monolithic photocatalysts can be prepared using various procedures, such as the extrusion of commercial nanopowders and binders [13], using sol-gel with titanium alkoxides, with or without templates [14-16], the impregnation of cordierite monoliths with titanium alkoxides and their subsequent calcination to fabricate an optical fiber honeycomb reactor [17], the impregnation of alumina monoliths with colloidal $TiO_2$ nanoparticles [18], the immersion of microchannel monoliths or transparent monoliths in sol-gel grown dispersions of nanoparticles (dip-coating) [19, 20], the chemical vapour deposition of $TiCl_4$ on silicon-coated substrates [21], etc. In recent years, a new method referred to as either liquid phase deposition (LPD) or sacrificial template accelerated hydrolysis (STAH) has been used to prepare $TiO_2$ nanorods, nanotubes or nanosheets on silicon-based, Fluorine doped Tin Oxide (FTO), Indium Tin Oxide (ITO) or stainless steel wire mesh (SSWM) substrates from templates based on non-polar ZnO nanorods [22-24] or polar ZnO nanosheets [25, 26]. Geometrical considerations suggest that the specific surface area of the materials derived from polar ZnO templates is much higher than that of the materials

consisting of nanorods or nanotubes, though until now only in one work by Vu et al. [26] has the specific surface area of the nanosheet-based material been reported (275 $m^2 g^{-1}$ on a $TiO_2$ mass basis). The very high surface area of this material and the flexibility of its monolithic support (micrometric stainless steel wire mesh) make it an ideal candidate for testing in photodegradation reactions of organic compounds in wastewaters, a process of paramount relevance from an environmental point of view.

In this work, we have tested for the first time high surface area SSWM-supported $TiO_2$ catalysts prepared by sacrificial template accelerated hydrolysis for the photodegradation of methylene blue in aqueous solutions under ultraviolet irradiation. Special attention has been focussed on the effect of the calcination temperature on the composition, texture and photodegradation activity of the catalysts.

## 2. Experimental

### 2.1. Preparation method

The support was a SSWM [with a wire diameter of 30 μm and a screen opening of 40 μm] provided by CISA Cedacería Industrial (www.cisa.net). The SSWM-supported ZnO was synthesized as described in [27]. To fabricate the titanium oxide the as-synthesized SSWM–supported ZnO templates were immersed in plastic flasks containing a 50 mL water solution of $K_2TiF_6$ (titanium to zinc molar ratio, $R_{Ti/Zn}$=1.5) and boric acid at a $H_3BO_3/K_2TiF_6$ molar ratio of 3/1. The closed flasks were subjected to shaking at RT in an orbital shaker for 1 day until a substitution degree of around 98% was achieved [26]. Afterwards, the samples were washed with deionized water, vacuum-dried at 60ºC for 30 min and calcined in air at a temperature in the 250-700°C range for 2 hours.

## 2.2. Material characterization

The chemical composition of the metal oxides was evaluated by means of atomic absorption spectroscopy. Scanning electron microscopy (SEM, FEI Quanta FEG 650 model) and transmission electron microscopy (TEM, JEM -2100F) were used to study the morphology of the samples. The X-ray diffraction (XRD) patterns of the catalysts were recorded on a Bruker D8 Advance instrument operating at 40 kV and 40 mA using Cu Kα radiation (λ = 0.15406 nm). Scherrer's equation was used to estimate the crystal size values ($d_{XRD}$) from the XRD pattern. The instrumental contribution to line broadening was considered. $N_2$ adsorption isotherms (-196ºC) obtained on a Micromeritics ASAP 2020 analyser were used to evaluate the BET specific surface area of the samples. UV-VIS diffuse reflectance spectroscopy measurements were carried out with selected samples using a Shimadzu UV-2460 spectrophotometer equipped with an integrating sphere. The spectra were recorded in the range of 200-700 nm. Pure $BaSO_4$ powder was used as a reference sample.

## 2.3. Photocatalytic tests

For the methylene blue photodegradation experiments the photocatalytic system shown in Figure 1 was used. Supported catalysts (1×5 $cm^2$ strips weighing ~100 mg) were tested in a 400 mL quartz beaker under the illumination of two ring-type UV 22W lamps (Luzchem Ring-Illuminator) which predominantly emit radiation at 351 nm with an incident flux density of $1.48\times10^{16}$ quanta $cm^{-3}$ $s^{-1}$. This parameter was evaluated by chemical actinometry [28]. The catalyst strip was held by a small clip fixed to the bottom of a vertical rod. The strip and the holder were immersed in an aqueous solution

of methylene blue (60 mL), with an initial concentration of 10 mg $L^{-1}$. The catalyst was then subjected to rotation at 120 r.p.m, firstly for 30 min under darkness to ensure adsorption/desorption equilibrium between the dye and the photocatalyst and then under the irradiation of the UV lamps for 120 min.

**[Figure 1]**

Liquid samples were extracted for measurement at set reaction times (0, 15, 30, 60, 90 and 120 min). The visible absorption peaks of the analyzed samples were recorded in the 400-800 nm range by means of a UV-Vis spectrometer (Shimadzu UV-2401PC). The true methylene blue concentration was obtained from the visible absorption spectra by means of a deconvolution technique [29] thereby making it possible to determine the contribution of the reaction intermediates to the spectra. For comparison purposes photocatalytic analyses were performed using either P25 $TiO_2$ powder or STAH $TiO_2$ powders scratched from selected wire mesh-supported $TiO_2$ samples. The powder (10 mg) was suspended in the magnetically stirred methylene blue solution for the photocatalytic experiment and the liquid samples subjected to analysis were previously centrifuged to remove the $TiO_2$ particles.

In order to compare the photocatalytic activity of the materials the catalytic activity parameter defined in [30], $A_C$ ($mg_{TiO2}^{-1}$ L $min^{-1}$), was used. From the equations that permit to evaluate this parameter under different conditions (Eqs. (9) to (12) in [30]) the correct form of equation (12) in [30] is the following:

$$A_C = \frac{b}{C_{C,0}\left\{1 - exp\left[\frac{C_{MB,0}^{1-n}(0.5^{1-n} - 1)\,b}{kC_{C,0}(1-n)}\right]\right\}} \quad (1)$$

in which the different variables are thoroughly described in [30]. Parameter $A_C$ allows the intrinsic activities of the catalysts to be compared on a $TiO_2$ mass basis using the same initial methylene blue concentration. In principle this parameter is independent of the catalyst dosage [30], although it is affected by mass transfer limitations and the quantum yield.

## 3. Discussion of results

### 3.1. Characterisation of the SSWM-supported $TiO_2$ catalysts

SSWM-supported $TiO_2$ samples were synthesised in this work following a sacrificial template accelerated hydrolysis procedure (STAH), a novel hard exotemplating technique that consists in forming metal oxide nanostructures via the hydrolysis of metal ions in the vicinity of a ZnO template [26, 31-33]. Hydrolysis is favoured by the removal of protons due to the simultaneous dissolution of the ZnO scaffold, which is the distinctive characteristic of this technique.

In previous works [26, 27] we synthesized a SSWM-supported ZnO material with a large proportion of polar surfaces [(100)/(002) XRD peaks ratio higher than 1]. This template displays a high specific surface area on a ZnO mass basis (80 $m^2\ g^{-1}$ in the case of samples calcined at 210ºC), a high yield (20.5 wt.%) and a good adhesion of the ZnO nanosheets to the SSWM support. When strongly or mildly acidic cations are used in aqueous solution in combination this ZnO template, the STAH technique can be applied to synthesize high surface area pure oxides ($TiO_2$, CuO, $CeO_2$, $\alpha$-$Fe_2O_3$) and these are obtained with a purity of over 95% and in high yields [26]. In the case of SSWM-supported $TiO_2$ we were able to produce samples with a 98% degree of purity, in average yields of 11.8±2.0 wt.% on the SSWM support for all samples and with a very

large specific surface area of 275 $m^2$ $g^{-1}$ (on a $TiO_2$ mass basis) in the case of the sample calcined at the lowest temperature (250°C). Figure 2 contains images of a SSWM-supported $TiO_2$ sample calcined at 250°C.

**[Figure 2]**

The morphology of the catalyst remained basically unchanged after the substitution process with respect to that of the ZnO template (compare the SEM images in Figure 2 with those reported in the previous literature [26, 27]). The white and flexible sample (photograph in Figure 2) is formed by $TiO_2$ homogeneously covering the SSWM in the form of arrays of thin nanosheets with a length distribution in the 5-7 μm range (SEM images), composed of nanograins 3-6 nm in size (TEM image) the stacking of which is responsible for the high porosity of the sample. Figure 3 shows the variation in specific surface area with the calcination temperature. There is a continuous decrease in the BET surface area with the increase in calcination temperature, though the surface area values are still very high. For instance, P25 $TiO_2$ powder calcined at 500°C for 2 hours has a specific surface area of 52 $m^2$ $g^{-1}$ [12], whereas, with the same calcination procedure, the SSWM-supported $TiO_2$ has a specific surface area of 87 $m^2$ $g^{-1}$.

**[Figure 3]**

XRD analyses were conducted to assess the effect of the calcination temperature on the crystal size and the anatase content of the SSWM-supported $TiO_2$ samples. Figure 4 shows the XRD plots for two samples calcined at 375 and 700°C. The crystal size

values were evaluated by applying Scherrer's equation to the (101) peak at 25.3°, whereas the anatase content was determined from the heights of the peaks corresponding to anatase ($I_a$, (101) peak at 25.3°) and rutile ($I_r$, (110) peak at 27.0-27.4°) using the equation in the figure [34, 35].

**[Figure 4]**

In the case of the samples with broader peaks (smaller crystal sizes) the overlapping peaks necessitated a deconvolution procedure to find the exact values of crystal size, $I_a$ and $I_r$, as illustrated by the curve for the sample calcined at 375°C (Figure 3). The rutile content of the samples was evaluated by subtracting the percentage of anatase from 100. Two samples were prepared at each calcination temperature and analysed by XRD according to the procedure explained above. Figure 5 shows the "apparent" rutile content and the crystal size ($d_{XRD}$) of all the samples analyzed. The qualifier "apparent" is used here for reasons that will be explained below.

**[Figure 5]**

Although rutile is thermodynamically stable in the whole temperature range [11], anatase is kinetically favoured at low temperatures. The sample calcined at the lowest temperature has a relatively high apparent rutile content (~9%). From this temperature up to 650°C the apparent rutile content decreases to a lower value range (3-8%). This observation contravenes the generally accepted rule that rutile cannot be transformed into anatase [11]. It should be noted however that the small, though conspicuous,

shoulders detected in XRD plots of the samples calcined at $T_c \leq 650°C$, ascribed initially to rutile, present an average maximum at 27.0±0.2°, well below the maximum at 27.4° detected for the sample calcined at 700°C (Figure 4). In addition the rutile crystal size is much smaller at $T_c \leq 650°C$ (7.4±2.6 nm) (randomly distributed over the temperature range) than at 700°C (18.6±1.3 nm). It is probable that what we have termed "apparent" rutile phase at $T_c \leq 650°C$ is really a solid solution of the residual ZnO (around 2 wt.%) and $TiO_2$, that has a crystal structure similar to that of rutile. This rutile-like phase may have formed during the room temperature synthesis of $TiO_2$ due to the well-known promotion effect that $Zn^{2+}$ has on the transformation of anatase to rutile [11, 36]. The possibility of synthesizing solid solutions of binary oxides at low temperature with the STAH method has already been pointed out in a previous work [26] and is currently an important topic of research in our laboratory. When the temperature is increased this phase probably splits into anatase and ZnO, which would explain its reduced presence on approaching 650°C. At 700°C the thermodynamic transformation of anatase to rutile becomes more evident, with the rutile content of the sample reaching a value of >20%. This temperature is higher than the transition onset temperature generally reported, which is around 600°C [11]. The relative amount of amorphous $TiO_2$ in the samples can be deduced from the degree of crystallinity (DOC), defined as the ratio of the (101) anatase peak height (subtracting the baseline) to the total height including the background of the XRD diffractogram [37]. We found that the DOC increased from 0.28 at 250°C to 0.45 at 450°C and to 0.59 at 700°C. Therefore, there is a significant presence of amorphous $TiO_2$ at 250°C.

With regards to the size of the anatase crystals, there is a clear increase from 6 to 10 nm in the 250-375°C temperature range (Figure 5), while at the same time there is a marked decrease in specific surface area from 275 to 126 $m^2 g^{-1}$ (Figure 3). From 375 to 450°C

a small, but clear, decrease in crystal size, from 10 to 8 nm is discernible. Then, after this local minimum, there is a continuous increase in anatase crystal size from ~8 (450°C) to ~21 nm (700°C).

To some extent the calcination temperature also affects the optical absorbance of the SSWM-supported $TiO_2$ catalysts. Figure 6 shows the DRS spectra corresponding to two SSWM-supported $TiO_2$ samples (calcined at 450 and 700°C) and P25 $TiO_2$ powder.

**[Figure 6]**

As can be seen for the region below 350 nm, the sample calcined at 700°C shows a slightly lower optical absorbance than P25 $TiO_2$ or the sample calcined at 450°C. The band gap energy values evaluated from the Kubelka-Munk absorption curves are 3.3, 3.3 and 3.2 eV, for the P25 $TiO_2$ particles and for the SSWM-supported samples calcined at 450 and 700°C, respectively.

### 3.2. Photocatalytic activity of the SSWM-supported $TiO_2$ catalysts

The main advantage of the photocatalysts prepared in this work is their monolithic configuration, which allows them to be retrieved from the reaction medium without the need for a costly separation stage (Figure 1). The micrometric stainless steel wire meshes are very flexible and can be rolled up to fit in the reaction chamber of a tubular micro-reactor, as described in [26, 38], or they can be fitted to rotating holders in batch reactors for the photodegradation of organic materials in water as in [27] and the present work. The kinetic results of the methylene blue photodegradation experiments conducted with the SSWM-supported $TiO_2$ catalysts or with the powdered catalysts

were mathematically processed using the equations in [30] (except equation (12) that is replaced by equation (1) in this work), as mentioned in the Experimental section, to obtain the intrinsic catalytic activity parameter, $A_C$, for the different catalysts. We used the equations for $n \neq 1$ to ensure a more accurate fitting of the experimental results. Figure 7 shows the variation of $A_C$ with the calcination temperature for the tests performed with the SSWM-supported catalysts fitted to a rotating holder immersed in the methylene blue solution.

**[Figure 7]**

The sample calcined at 250°C, which is a mixture of anatase, amorphous $TiO_2$ and a small amount of what we have described as a ZnO-$TiO_2$ solid solution with a crystal structure similar to that of rutile, presents a relatively high catalytic activity, which is ascribed to its large specific surface area (275 $m^2 g^{-1}$). At 375°C, the specific surface area of the sample has been halved, to a value of 126 $m^2 g^{-1}$, with a concomitant decrease in the number of active centers for photocatalysis. This explains the marked reduction in catalytic activity with respect to the sample calcined at 250°C (Figure 7). From 375 to 400°C there is a notable increase in catalytic activity, which is coincident with a slight diminution of anatase crystal size (Figure 5). We attribute this to the transformation of amorphous $TiO_2$ to crystalline anatase of small crystal size. The average crystal size of the anatase phase in this temperature region is derived from the combination of the crystal size of the anatase resulting from the room temperature synthesis, which increases with the rise in temperature from 250 to 375°C in a typical sintering phenomenon (Figure 5), and the small crystal size of the anatase resulting from the transformation of amorphous $TiO_2$. This explains the unexpected diminution in

size of the anatase crystals and the marked increase in catalytic activity, which is undoubtedly a consequence of the higher degree of crystallinity in the anatase phase. From 450 to 600°C there is a slight decrease in the catalytic activity, which is attributed to a diminution of specific surface area (from 91 to ~51 $m^2 g^{-1}$) and a parallel increment in anatase crystal size (from 8 to 14 nm) due to sintering. This temperature region, which has been highlighted in Figure 7 by a grey shadow, is considered to be the optimal region of calcination for preparing the catalysts destined for the photodegradation of methylene blue. From 600 to 650°C there is a notable decrease in catalytic activity, which cannot be ascribed to any marked change in specific surface area (Figure 3), anatase crystal size or apparent rutile content (Figure 5). However, it is well known that the onset of the transformation from anatase to rutile occurs at around 600°C [11] in a nucleation process at anatase (112) twin boundaries [39], and therefore the rutile nuclei that are formed around the anatase crystals might alter their photocatalytic properties before the amount of the rutile phase surpases the detection limit of the X-Ray diffractometer. It is for this reason that the decrease in catalytic activity from 600 to 650°C is ascribed to the onset of rutile formation, as indicated in Figure 7. A further decrease in catalytic activity at temperatures over 650°C is attributed to the presence of rutile (over 20%) and a decrease in the number of active centers in the anatase phase when $d_{XRD}$ increases and $S_{BET}$ decreases.

For comparison purposes, 10 mg of powder scratched from the most active SSWM-supported catalysts (STAH $TiO_2$; $T_c$=450 and 500°C) and 10 mg of P25 $TiO_2$ were tested in the batch photodegradation of methylene blue under the same experimental conditions. Figure 8 shows the decay of the methylene blue concentration corresponding to the three catalysts.

**[Figure 8]**

By comparing the $A_C$ values in Figure 7, obtained from equation 11 in [30], with those in Figure 8, it can be deduced that the catalytic activity of SSWM-supported catalysts with a monolithic configuration is around 30% that of the particles scratched from the surface of the stainless steel wire mesh. This is due to the fact that the loose particles are more evenly distributed in the liquid, which is beneficial for the mass transfer of methylene blue to the active centers of the catalyst and, undoubtedly, for the usage of a larger fraction of the UV irradiation. In this work we employed a simple set-up for testing monolithic catalysts consisting of a wire mesh strip rotating inside the liquid bulk, as described in the Experimental section (Figure 1). Other configurations based on quartz micro-reactors that reduce the mass transfer path and increase the usage of UV irradiation are to be tested in the near future.

As can be seen in Figure 8, the STAH $TiO_2$ samples prepared in this work are more active than the P25 $TiO_2$ particles. The $A_C$ values in the figure indicate that the $TiO_2$ particles prepared by STAH and calcined at 450°C show twice the catalytic activity for the photodegradation of methylene blue in an aqueous solution than the P25 $TiO_2$ particles. The superiority of the STAH-prepared particles can be ascribed to their larger specific surface area and smaller rutile content with respect to the P25 $TiO_2$ particles (i.e., a higher density of anatase active centers) for the same degree of crystallinity (the same calcination temperature).

## 4. Conclusions

Stainless steel wire mesh-supported $TiO_2$ catalysts were prepared by sacrificial template accelerated hydrolysis using highly polar SSWM-supported ZnO templates. The calcination temperature of the catalysts significantly affects the composition, crystallinity, the textural properties and the photocatalytic activity of the catalysts. Thus, at 250°C the catalyst, which is mainly composed of anatase and amorphous $TiO_2$ and, to a lesser extent, a ZnO-$TiO_2$ rutile-like solid solution, the amount of which decreases with the increase in the calcination temperature, has a high specific surface area (275 $m^2\ g^{-1}$) and shows a remarkable catalytic activity for the photodegradation of methylene blue in aqueous solution. At 375°C the anatase crystal size has grown considerably and both the specific surface area and the catalytic activity have experienced a parallel decrease. In the 375-450°C range the transformation of amorphous $TiO_2$ into small anatase crystals provokes a diminution in anatase crystal size and a marked increase in catalytic activity, which reaches its highest value at 450°C. From this temperature to 600°C the catalytic activity undergoes a gradual reduction as a consequence of the loss of active centers due to sintering. Beyond 600°C the reduction in catalytic activity is more severe, as a consequence of the onset of rutile formation. The most active catalyst prepared in this work shows a catalytic activity which is twice that of the reference catalyst P25 $TiO_2$.

**Acknowledgements**

The financial support for this research work provided by the Spanish MEC (CTQ2011-24776) is gratefully acknowledged. Tan T. Vu is grateful to the CSIC for the award of a JAE predoc grant.

Reference list

[1] Y. Huang, G. Pandraud, P.M. Sarro, Reflectance-based $TiO_2$ photonic crystal sensors, in: Solid-State Sensors, Actuators and Microsystems Conference (TRANSDUCERS), 2011 16th International, 2011, pp. 2682-2685.

[2] L. Xiong, J. Li, Y. Yu, Energy Storage in Bifunctional TiO2 Composite Materials under UV and Visible Light, Energies, 2 (2009) 1009-1030.

[3] N. Li, G. Liu, C. Zhen, F. Li, L. Zhang, H.-M. Cheng, Battery Performance and Photocatalytic Activity of Mesoporous Anatase TiO2 Nanospheres/Graphene Composites by Template-Free Self-Assembly, Advanced Functional Materials, 21 (2011) 1717-1722.

[4] E. Lancelle-Beltran, P. Prené, C. Boscher, P. Belleville, P. Buvat, C. Sanchez, All-Solid-State Dye-Sensitized Nanoporous TiO2 Hybrid Solar Cells with High Energy-Conversion Efficiency, Advanced Materials, 18 (2006) 2579-2582.

[5] R. Vogel, P. Meredith, I. Kartini, M. Harvey, J.D. Riches, A. Bishop, N. Heckenberg, M. Trau, H. Rubinsztein-Dunlop, Mesostructured Dye-Doped Titanium Dioxide for Micro-Optoelectronic Applications, Chemphyschem, 4 (2003) 595-603.

[6] A. Fujishima, K. Honda, Electrochemical Photolysis of Water at a Semiconductor Electrode, Nature, 238 (1972) 37-38.

[7] G. Lui, J.-Y. Liao, A. Duan, Z. Zhang, M. Fowler, A. Yu, Graphene-wrapped hierarchical TiO2 nanoflower composites with enhanced photocatalytic performance, Journal of Materials Chemistry A, 1 (2013) 12255-12262.

[8] M.A. Fox, M.T. Dulay, Heterogeneous Photocatalysis, Chemical Reviews, 93 (1993) 341-357.

[9] A. Sclafani, J.M. Herrmann, Comparison of the Photoelectronic and Photocatalytic Activities of Various Anatase and Rutile Forms of Titania in Pure Liquid Organic Phases and in Aqueous Solutions, The Journal of Physical Chemistry, 100 (1996) 13655-13661.

[10] C. He, B. Tian, J. Zhang, Thermally stable $SiO_2$-doped mesoporous anatase $TiO_2$ with large surface area and excellent photocatalytic activity, Journal of Colloid and Interface Science, 344 (2010) 382-389.

[11] D.H. Hanaor, C. Sorrell, Review of the anatase to rutile phase transformation, Journal of Materials Science, 46 (2011) 855-874.

[12] K.J.A. Raj, B. Viswanathan, Effect of surface area, pore volume and particle size of P25 titania on the phase transformation of anatase to rutile, Indian Journal of Chemistry, 48A (2009) 1378-1382.

[13] P. Avila, A. Bahamonde, J. Blanco, B. Sánchez, A.I. Cardona, M. Romero, Gas-phase photo-assisted mineralization of volatile organic compounds by monolithic titania catalysts, Applied Catalysis B: Environmental, 17 (1998) 75-88.

[14] O. Ruzimuradov, S. Nurmanov, M. Hojamberdiev, R.M. Prasad, A. Gurlo, J. Broetz, K. Nakanishi, R. Riedel, Fabrication of nitrogen-doped TiO2 monolith with well-defined macroporous and bicrystalline framework and its photocatalytic performance under visible light, Journal of the European Ceramic Society, 34 (2014) 809-816.

[15] O. Ruzimuradov, S. Nurmanov, M. Hojamberdiev, R.M. Prasad, A. Gurlo, J. Broetz, K. Nakanishi, R. Riedel, Preparation and characterization of macroporous TiO2–SrTiO3 heterostructured monolithic photocatalyst, Materials Letters, 116 (2014) 353-355.

[16] J. Du, H. Chen, H. Yang, R. Sang, Y. Qian, Y. Li, G. Zhu, Y. Mao, W. He, D.J. Kang, A facile sol–gel method for synthesis of porous Nd-doped TiO2 monolith with enhanced photocatalytic activity under UV–Vis irradiation, Microporous and Mesoporous Materials, 182 (2013) 87-94.

[17] E. Taboada, I. Angurell, J. Llorca, Dynamic photocatalytic hydrogen production from ethanol-water mixtures in an optical fiber honeycomb reactor loaded with $Au/TiO_2$, Journal of Catalysis, 309 (2014) 460-467.

[18] Z. Jia, M. Bouslama, M.B. Amar, M. Amamra, M. Kayse, M. Traore, S. Tieng, K. Chhor, A. Chianese, V. Nadtochenko, A. Kanaev, Nanoparticulate media for environmental applications, Funcional Materials, 20 (2013) 417-423.

[19] M. Tahir, N.S. Amin, Photocatalytic CO2 reduction and kinetic study over In/TiO2 nanoparticles supported microchannel monolith photoreactor, Applied Catalysis A: General, 467 (2013) 483-496.

[20] F.V.S. Lopes, S.M. Miranda, R.A.R. Monteiro, S.D.S. Martins, A.M.T. Silva, J.L. Faria, R.A.R. Boaventura, V.J.P. Vilar, Perchloroethylene gas-phase degradation over titania-coated transparent monoliths, Applied Catalysis B: Environmental, 140–141 (2013) 444-456.

[21] W.-J. Lee, Y.-M. Sung, Synthesis of Anatase Nanosheets with Exposed (001) Facets via Chemical Vapor Deposition, Crystal Growth & Design, 12 (2012) 5792-5795.

[22] J.H. Lee, I.C. Leu, M.C. Hsu, Y.W. Chung, M.H. Hon, Fabrication of Aligned $TiO_2$ One-Dimensional Nanostructured Arrays Using a One-Step Templating Solution Approach, The Journal of Physical Chemistry B, 109 (2005) 13056-13059.

[23] T. Rattanavoravipa, T. Sagawa, S. Yoshikawa, Photovoltaic performance of hybrid solar cell with $TiO_2$ nanotubes arrays fabricated through liquid deposition using ZnO template, Solar Energy Materials and Solar Cells, 92 (2008) 1445-1449.

[24] S. Yodyingyong, X. Zhou, Q. Zhang, D. Triampo, J. Xi, K. Park, B. Limketkai, G. Cao, Enhanced Photovoltaic Performance of Nanostructured Hybrid Solar Cell Using Highly Oriented $TiO_2$ Nanotubes, The Journal of Physical Chemistry C, 114 (2010) 21851-21855.

[25] J.J. Yuan, H.D. Li, Q.L. Wang, Q. Yu, X.K. Zhang, H.J. Yu, Y.M. Xie, Fabrication, characterization, and photocatalytic activity of double-layer TiO2 nanosheet films, Materials Letters, 81 (2012) 123-126.

[26] T.T. Vu, G. Marbán, Sacrificial template synthesis of high surface area metal oxides. Example: An excellent structured Fenton-like catalyst, Applied Catalysis B: Environmental, 152–153 (2014) 51-58.

[27] T.T. Vu, L. del Río, T. Valdés-Solís, G. Marbán, Fabrication of wire mesh-supported ZnO photocatalysts protected against photocorrosion, Applied Catalysis B: Environmental, 140–141 (2013) 189-198.

[28] C.G. Hatchard, C.A. Parker, A New Sensitive Chemical Actinometer. II. Potassium Ferrioxalate as a Standard Chemical Actinometer, Proceedings of the Royal Society of London. Series A. Math.l and Phys. Sciences, 235 (1956) 518-536.

[29] G. Marbán, T.T. Vu, T. Valdés-Solís, Simple spectrum deconvolution technique to avoid the artifact induced by the hypsochromic shift masking the concentration of methylene blue analyzed by visible spectroscopy during photodegradation experiments, Applied Catalysis A: General, 402 (2011) 218-223.

[30] T.T. Vu, L. del Río, T. Valdés-Solís, G. Marbán, Stainless steel wire mesh-supported ZnO for the catalytic photodegradation of methylene blue under ultraviolet irradiation, Journal of Hazardous Materials, 246-247 (2013) 126-134.

[31] J. Liu, Y. Li, H. Fan, Z. Zhu, J. Jiang, R. Ding, Y. Hu, X. Huang, Iron Oxide-Based Nanotube Arrays Derived from Sacrificial Template-Accelerated Hydrolysis: Large-Area Design and Reversible Lithium Storage, Chemistry of Materials, 22 (2010) 212-217.

[32] L. Qin, Q. Zhu, G. Li, F. Liu, Q. Pan, Controlled fabrication of flower-like ZnO-$Fe_2O_3$ nanostructured films with excellent lithium storage properties through a partly sacrificed template method, Journal of Materials Chemistry, 22 (2012) 7544-7550.

[33] W. Zeng, F. Zheng, R. Li, Y. Zhan, Y. Li, J. Liu, Template synthesis of $SnO_2$/$\alpha$-$Fe_2O_3$ nanotube array for 3D lithium ion battery anode with large areal capacity, Nanoscale, 4 (2012) 2760-2765.

[34] G. Colón, J.M. Sánchez-España, M.C. Hidalgo, J.A. Navío, Effect of TiO2 acidic pre-treatment on the photocatalytic properties for phenol degradation, Journal of Photochemistry and Photobiology A: Chemistry, 179 (2006) 20-27.

[35] T.L. Thompson, J.T. Yates, Surface Science Studies of the Photoactivation of TiO2New Photochemical Processes, Chemical Reviews, 106 (2006) 4428-4453.

[36] N. Bamba, S. Kuribara, T. Fukami, $TiO_2$ - ZnO Porous Films Formed by ZnO Dissolution, Advances in Technology of Materials and Materials Processing Journal, 9 (2007) 55-58.

[37] I. López, T. Valdés-Solís, G. Marbán, Highly Active Cobalt Oxide Catalysts Prepared by SACOP for the Preferential Oxidation of CO in Excess Hydrogen, ChemCatChem, 3 (2011) 734-740.

[38] G. Marbán, A. López, I. López, T. Valdés-Solís, A highly active, selective and stable copper/cobalt-structured nanocatalyst for methanol decomposition, Applied Catalysis B: Environmental, 99 (2010) 257-264.

[39] H.-H. Ko, H.-T. Chen, F.-L. Yen, W.-C. Lu, C.-W. Kuo, M.-C. Wang, Preparation of TiO2 Nanocrystallite Powders Coated with 9 mol% ZnO for Cosmetic Applications in Sunscreens, International Journal of Molecular Sciences, 13 (2012) 1658-1669.

**Captions to figures**

**Figure 1.** Images of the photocatalytic system: a) Photocatalytic reactor, b) detail of the catalyst strip and the rotatory holder, c) reactor vessel and ring-type lamps

**Figure 2.** Photography, SEM images and a TEM image of a SSWM-supported $TiO_2$ sample calcined at 250°C

**Figure 3.** Variation of the specific surface area (on a $TiO_2$ mass basis) of the SSWM-supported $TiO_2$ samples with the calcination temperature

**Figure 4.** XRD plots for SSWM-supported $TiO_2$ calcined at 375 and 700°C, and the method of calculating the anatase percentage from the height of the peaks

**Figure 5.** Variation of the and apparent rutile content and the anatase crystal size ($d_{XRD}$) with the calcination temperature of the SSWM-supported $TiO_2$ catalysts

**Figure 6.** Diffuse reflectance spectra (DRS) of the SSWM-supported $TiO_2$ catalysts (calcined at 450 and 700°C) and P25 $TiO_2$ particles

**Figure 7.** Variation of the catalytic activity ($A_C$) with the calcination temperature for the SSWM-supported catalysts fitted to a rotating holder immersed in the methylene blue solution

**Figure 8.** Methylene blue concentration decay curves for the particulate samples scratched from the SSWM-supported $TiO_2$ catalysts (calcined at 450 and 500°C) and the P25 $TiO_2$ particles. The values of $A_C$ for the different catalysts are also included in the figure

**Figures**

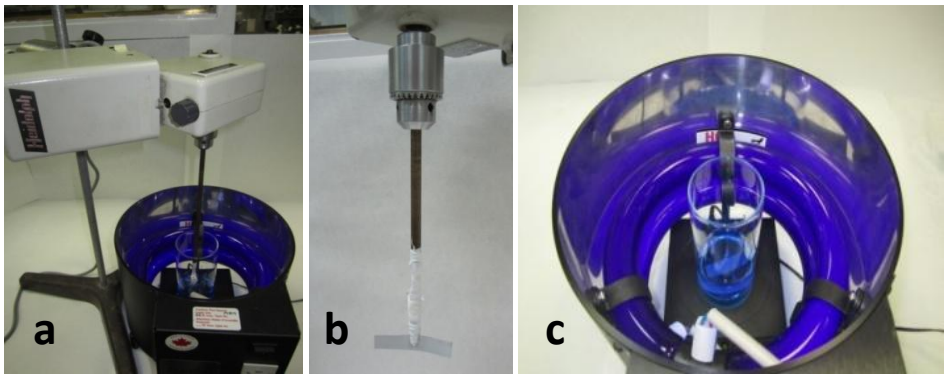


Figure 1

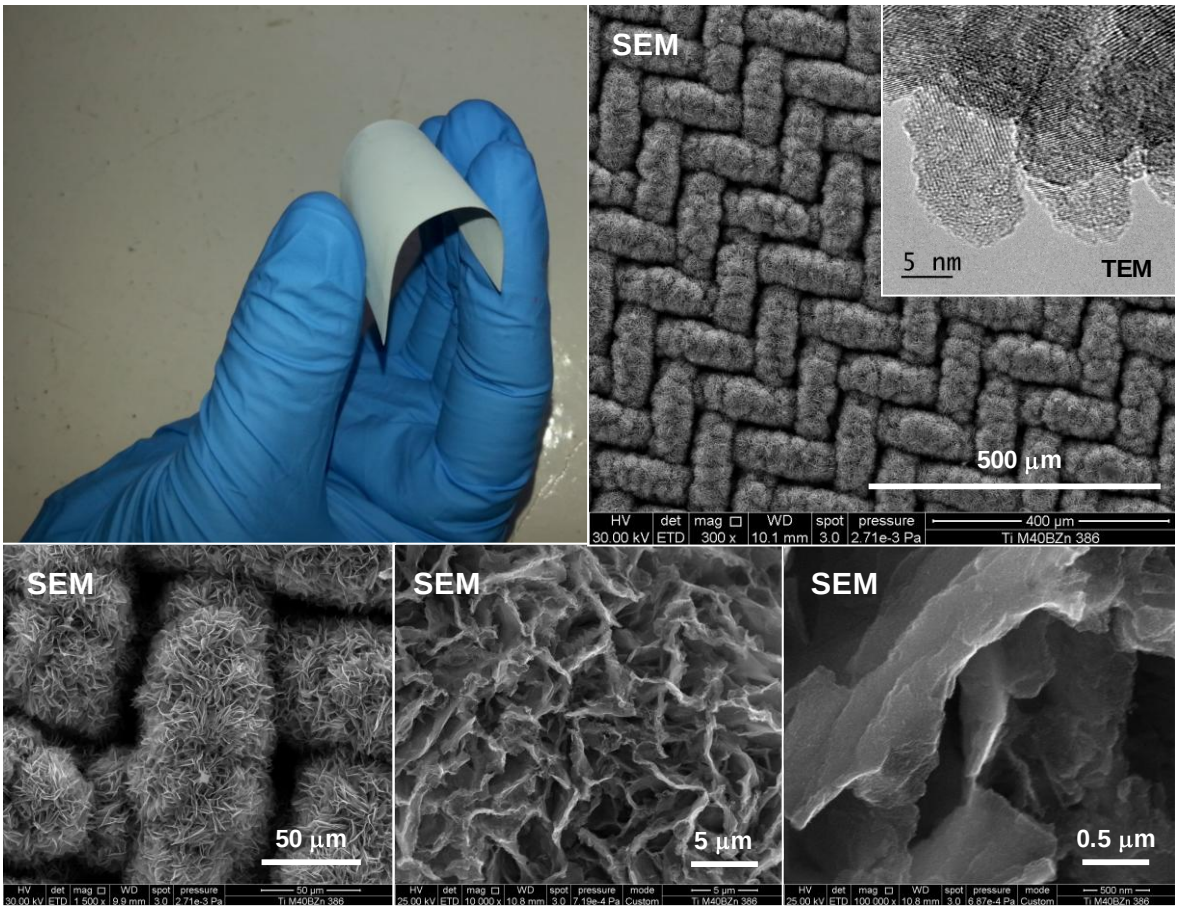
SEM
500 µm
HV
30.00 kV
det
ETD
mag
300 x
WD
10.1 mm
spot
3.0
pressure
2.71e-3 Pa
400 µm
Ti M40BZn 386
5 nm
TEM
SEM
50 µm
SEM
5 µm
SEM
0.5 µm

Figure 2

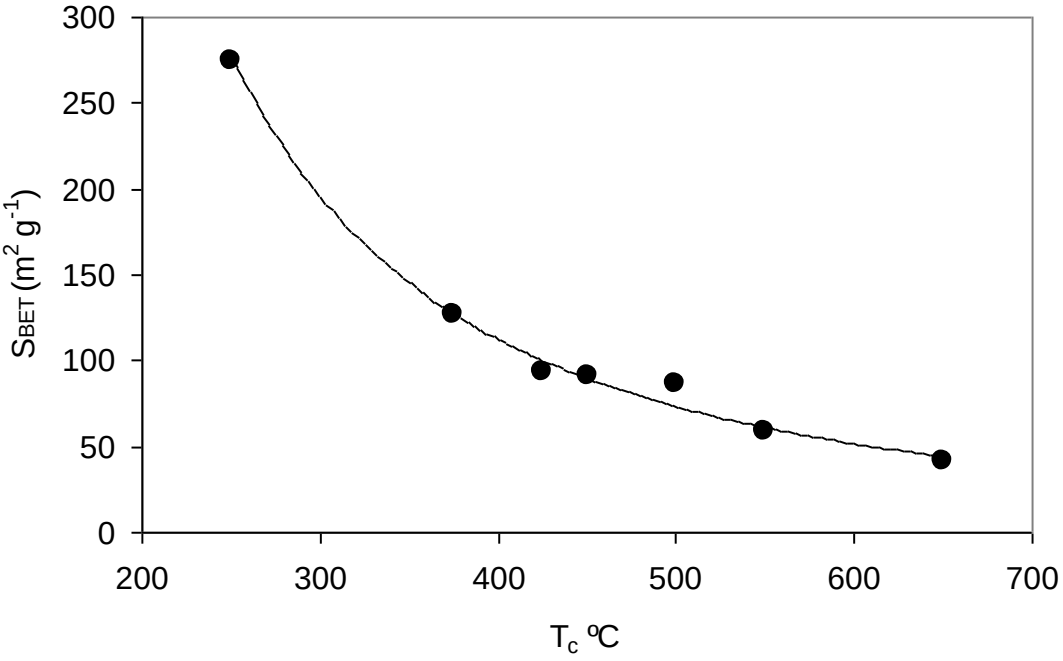


Figure 3

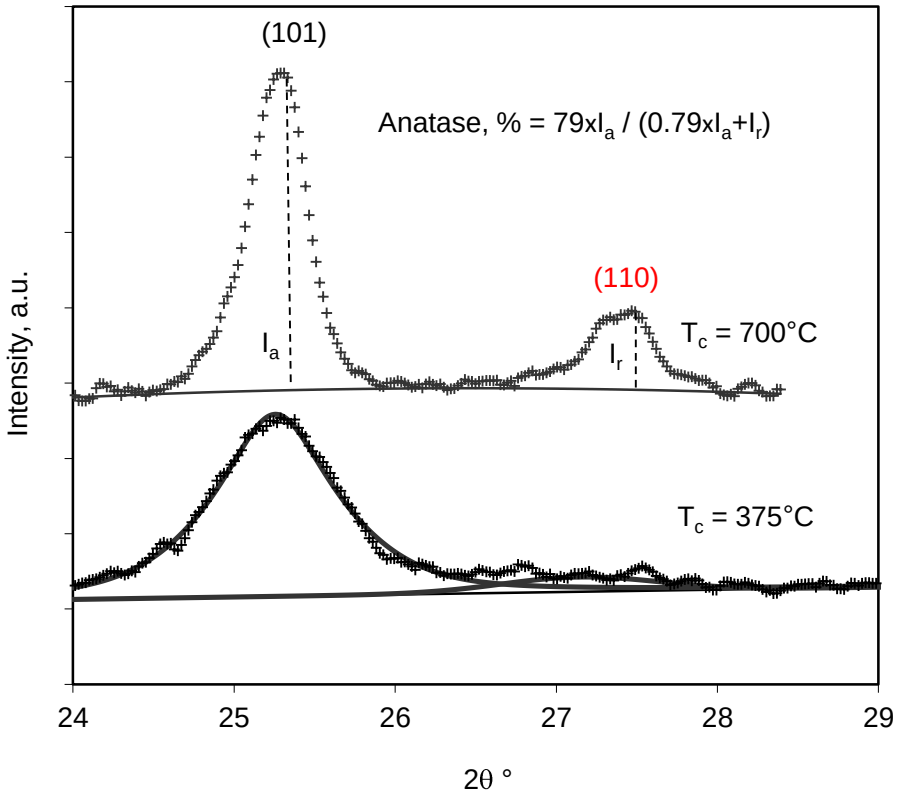
(101)
Anatase, % = 79xI$_a$ / (0.79xI$_a$+I$_r$)
(110)
I$_a$
I$_r$
T$_c$ = 700°C
T$_c$ = 375°C
Intensity, a.u.
24
25
26
27
28
29
2θ °

Figure 4

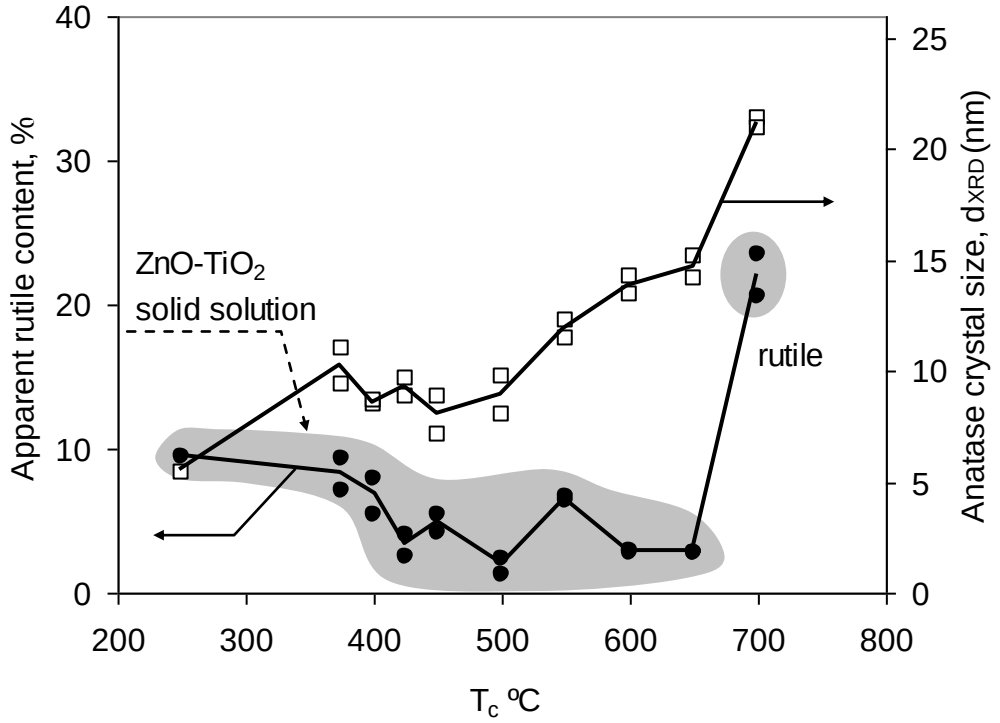
40
30
20
10
0
25
20
15
10
5
0
200
300
400
500
600
700
800
Apparent rutile content, %
Anatase crystal size, dXRD (nm)
Tc ºC
ZnO-TiO2
solid solution
rutile

Figure 5

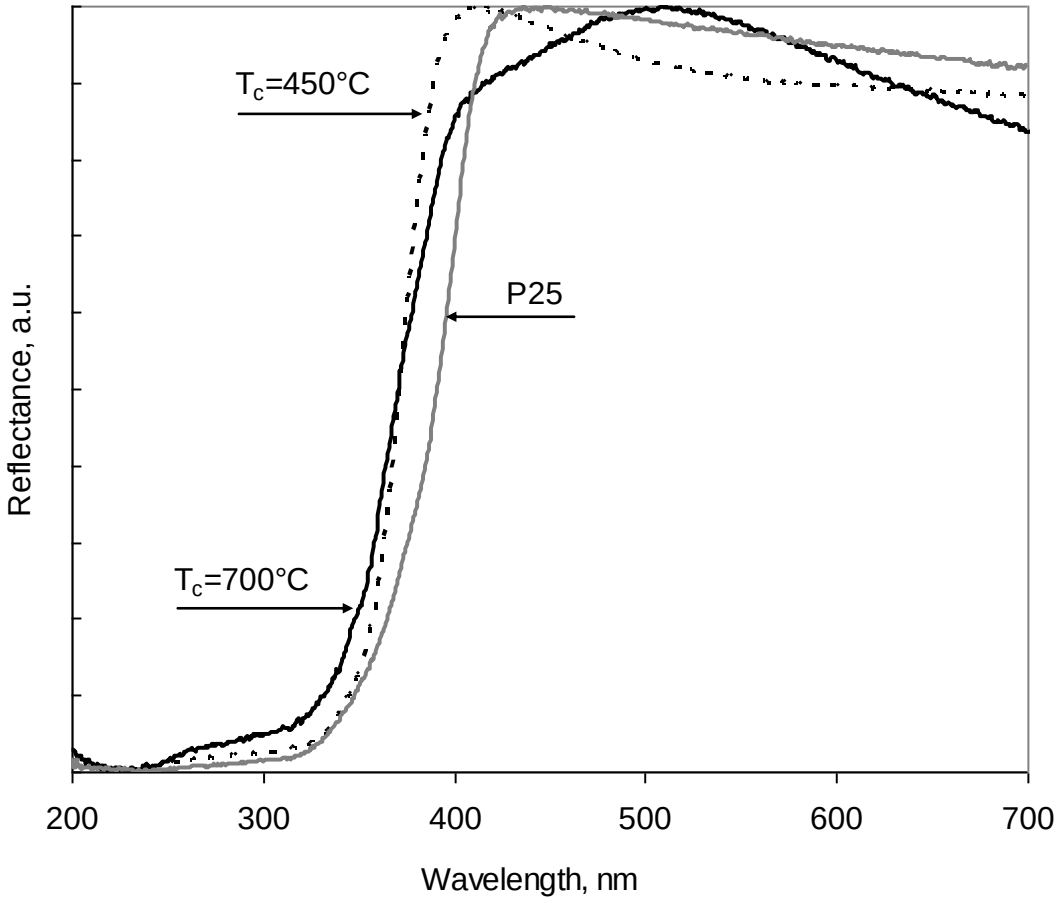
Reflectance, a.u.
Wavelength, nm
200
300
400
500
600
700
T$_c$=450°C
P25
T$_c$=700°C

Figure 6

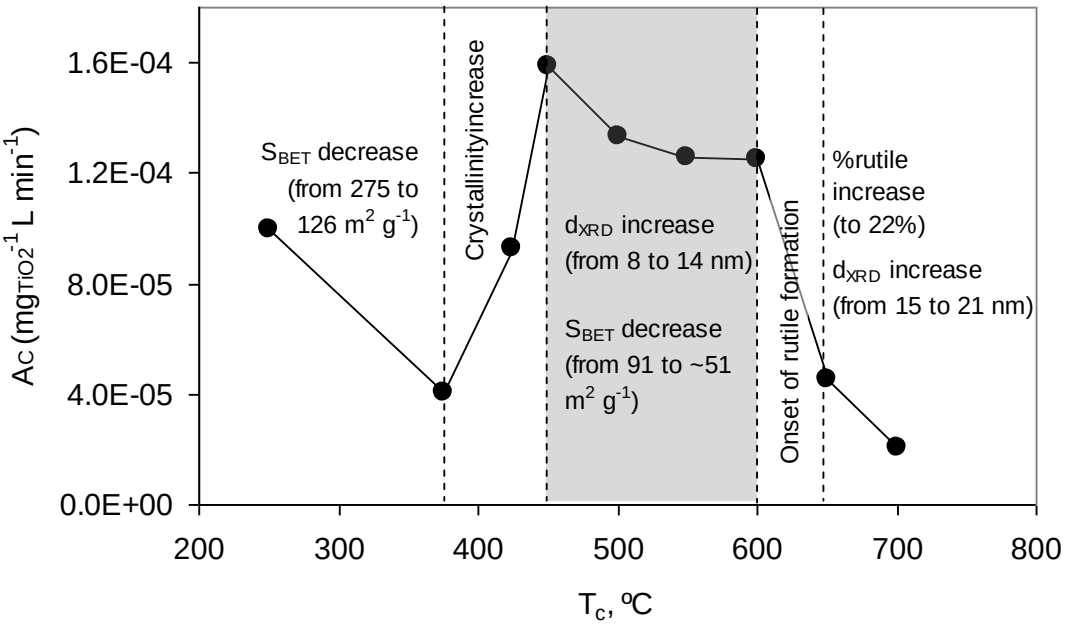
1.6E-04
1.2E-04
8.0E-05
4.0E-05
0.0E+00
Ac (mgTiO2-1 L min-1)
200
300
400
500
600
700
800
Tc, ºC
SBET decrease
(from 275 to
126 m2 g-1)
Crystallinityincrease
dXRD increase
(from 8 to 14 nm)
SBET decrease
(from 91 to ~51
m2 g-1)
Onset of rutile formation
%rutile
increase
(to 22%)
dXRD increase
(from 15 to 21 nm)

Figure 7

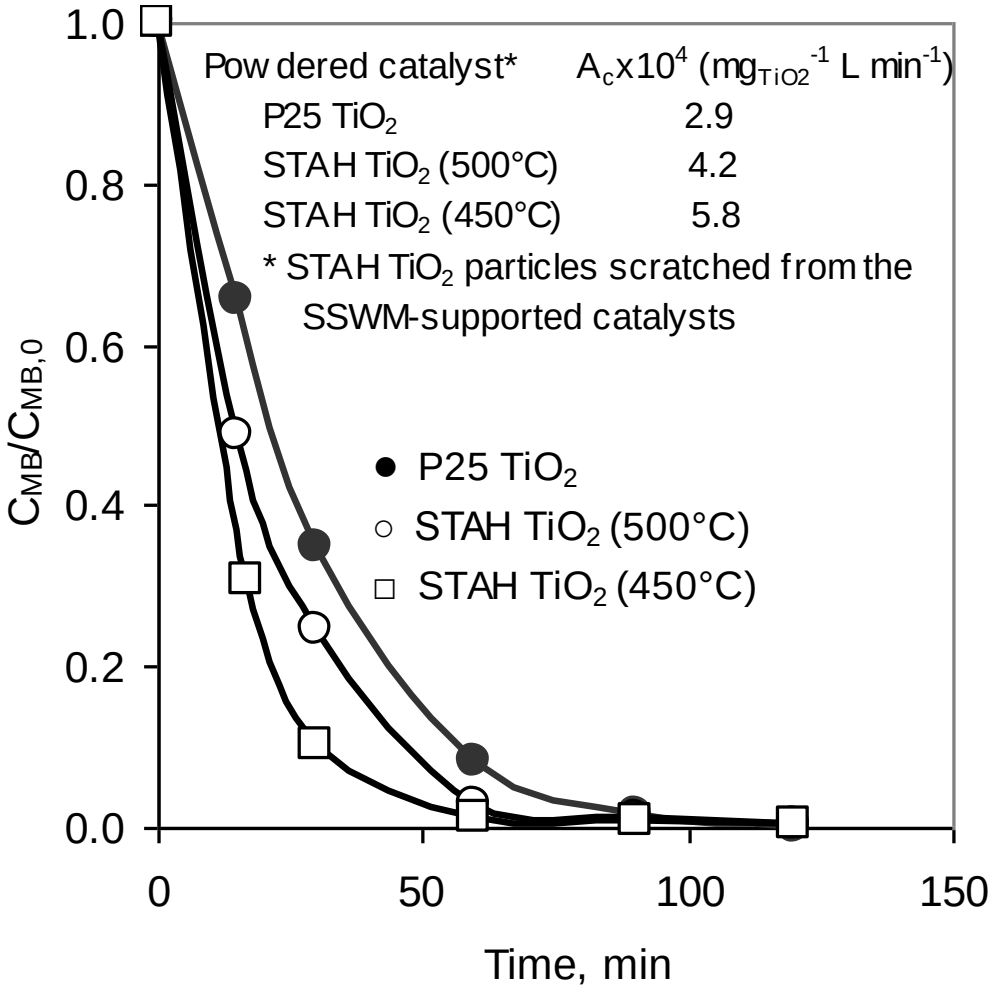
Powdered catalyst*
$A_c x10^4$ ($mg_{TiO2}^{-1}$ L $min^{-1}$)
P25 $TiO_2$ 2.9
STAH $TiO_2$ (500°C) 4.2
STAH $TiO_2$ (450°C) 5.8
* STAH $TiO_2$ particles scratched from the SSWM-supported catalysts
P25 $TiO_2$
STAH $TiO_2$ (500°C)
STAH $TiO_2$ (450°C)
$C_{MB}/C_{MB,0}$
1.0
0.8
0.6
0.4
0.2
0.0
0
50
100
150
Time, min

Figure 8